Received: 23 December 2017 | Revised: 1 July 2019 | Accepted: 2 July 2019

DOI: 10.1111/epi.16296

FULL-LENGTH ORIGINAL RESEARCH

Epilepsia®

Increased gamma and decreased fast ripple connections of epileptic tissue: A high-frequency directed network approach

Willemiek J. E. M. Zweiphenning[1] | **Hanneke M. Keijzer**[1,2] | **Eric van Diessen**[3] | **Maryse A. van 't Klooster**[1] | **Nicole E. C. van Klink**[1] | **Frans S. S. Leijten**[1] | **Peter C. van Rijen**[1] | **Michel J. A. M. van Putten**[2] | **Kees P. J. Braun**[3] | **Maeike Zijlmans**[1,4]

[1]Department of Neurology and Neurosurgery, University Medical Center Utrecht Brain Center, Utrecht University, Utrecht, the Netherlands

[2]MIRA Institute for Biomedical Technology and Technical Medicine, Clinical Neurophysiology Group, University of Twente, Enschede, the Netherlands

[3]Department of Pediatric Neurology, University Medical Center Utrecht Brain Center, Utrecht University, Utrecht, the Netherlands

[4]Epilepsy Foundation of the Netherlands, Heemstede, the Netherlands

Correspondence
Willemiek J. E. M. Zweiphenning, Department of Neurology and Neurosurgery, University Medical Center Utrecht, HP C03.1.31, Heidelberglaan 100, 3584 CX Utrecht, the Netherlands.
Email: W.J.E.Zweiphenning@umcutrecht.nl

Funding information
UMC Utrecht Alexandre Suerman MD/PhD Stipendium 2015; Dutch Epilepsy Foundation, Grant/Award Number: 2012-04 and 2015-09; Dutch Brain Foundation, Grant/Award Number: 2013-139; ZonMW-VENI, Grant/Award Number: 91615149

Abstract

Objective: New insights into high-frequency electroencephalographic activity and network analysis provide potential tools to improve delineation of epileptic tissue and increase the chance of postoperative seizure freedom. Based on our observation of high-frequency oscillations "spreading outward" from the epileptic source, we hypothesize that measures of directed connectivity in the high-frequency range distinguish epileptic from healthy brain tissue.

Methods: We retrospectively selected refractory epilepsy patients with a malformation of cortical development or tumor World Health Organization grade I/II who underwent epilepsy surgery with intraoperative electrocorticography for tailoring the resection based on spikes. We assessed directed functional connectivity in the theta (4-8 Hz), gamma (30-80 Hz), ripple (80-250 Hz), and fast ripple (FR; 250-500 Hz) bands using the short-time direct directed transfer function, and calculated the total, incoming, and outgoing propagation strength for each electrode. We compared network measures of electrodes covering the resected and nonresected areas separately for patients with good and poor outcome, and of electrodes with and without spikes, ripples, and FRs (group level: paired *t* test; patient level: Mann-Whitney *U* test). We selected the measure that could best identify the resected area and channels with epileptic events using the area under the receiver operating characteristic curve, and calculated the positive and negative predictive value, sensitivity, and specificity.

Results: We found higher total and outstrength in the ripple and gamma bands in resected tissue in patients with good outcome ($ripple_{total}$: $P = .01$; $ripple_{out}$: $P = .04$; $gamma_{total}$: $P = .01$; $gamma_{out}$: $P = .01$). Channels with events showed lower total and instrength, and higher outstrength in the FR band, and higher total and outstrength in the ripple, gamma, and theta bands (FR_{total}: $P = .05$; FR_{in}: $P < .01$; FR_{out}: $P = .02$; $gamma_{total}$: $P < .01$; $gamma_{in}$: $P = .01$; $gamma_{out}$: $P < .01$; $theta_{total}$: $P = .01$; $theta_{out}$: $P = .01$). The total strength in the gamma band was most distinctive at the channel level (positive predictive value $[PPV]_{good} = 74\%$, $PPV_{poor} = 43\%$).

Significance: Interictally, epileptic tissue is isolated in the FR band and acts as a driver up to the (fast) ripple frequency range. The gamma band total strength seems promising to delineate epileptic tissue intraoperatively.

KEYWORDS
effective connectivity, epilepsy, epilepsy surgery, high-frequency activity, high-frequency oscillations, network analysis

1 | INTRODUCTION

Despite attempts to delineate the epileptic tissue with spikes and spike patterns in intraoperative electrocorticography (ioECoG), approximately one-quarter of patients are not seizure-free 2 years after epilepsy surgery.[1] Over the past decade, high-frequency oscillations (HFOs) have been designated as promising biomarkers for epilepsy. HFOs are transient bursts of activity above the frequency that is normally reviewed in clinical electroencephalography (EEG) and are subdivided into ripples (80-250 Hz) and fast ripples (FRs; 250-500 Hz).[2] HFOs correlate better with the seizure onset zone (SOZ) and with postsurgical outcome than epileptic spikes,[2–5] and are linked to seizure rate and treatment response.[6]

An equally intriguing insight is the recent view of focal epilepsy as a network disorder with aberrant connectivity at different scales. At the microscale, abnormal neuronal connections are involved in HFO generation.[7,8] At the mesoscale, the coordinated activity across several centimeters of neocortex explains the signs and symptoms during focal seizures.[9,10] At the macroscale, disrupted whole brain interactions explain the observed cognitive and behavioral symptoms not necessarily associated with the location of the epileptic focus.[11–13]

Brain networks can be defined at the level of synchronicity between brain areas, named functional connectivity.[10,14,15] Functional connectivity can be computed in numerous ways; each approach quantifies different aspects of (changes in) neuronal interactions. It can be based on linear or nonlinear interactions, with or without taking directionality into account.[16,17] Functional network analysis constructs a map of the brain with the recording sites as nodes and the interaction between signals measured at different recording sites as edges. Local network measures subsequently characterize each node within the network, indicating its importance or "centrality" for functional interactions between brain areas.[10,14,15]

Intracranial EEG studies in focal epilepsy patients increasingly investigate mesoscale local network measures to improve delineation of the epileptic tissue.[18–31] In the conventional frequency bands (up to 80 Hz), the epileptic tissue is generally characterized as a strongly connected region or "hub" node in the network,[18,19,29] or as a "source" or "driver" allowing epileptic activity to spread to other regions when directed measures are used.[20,24–26,31] Including the node with the highest centrality measure in the resection correlates with postsurgical seizure freedom.[24–26,29] Recent studies combining functional network analysis and HFOs found isolation of areas displaying interictal HFO events in the gamma band,[21,23,27] and (pre)ictal high gamma and ripple outflow from the SOZ and its vicinity starting before the first visible EEG changes.[22,30]

We occasionally observe propagation of HFOs across distinct but still spatially confined cortical areas at times when epileptic spikes are widespread (Figure 1). These observations, together with the idea of focal epilepsy being the result of aberrant connectivity at different scales, led us to the hypothesis that propagating HFOs may be the mesoscale silhouette of an underlying microscale HFO-generating network, and that directed connectivity in the high-frequency ranges can discriminate epileptic from healthy tissue in the operating theater. We therefore aimed to discriminate epileptic from healthy brain tissue by comparing high-frequency directed network measures between the resected and nonresected areas and between channels with and without events in lesional focal epilepsy patients who did or did not become seizure-free after traditional ioECoG-tailored resective surgery.

Key Points

- Resected area of patients who are seizure-free after surgery shows more outgoing propagations in ripple and gamma band preresection ioECoG
- Channels with epileptic events show fewer total and incoming, and more outgoing propagations in the fast ripple band than channels without
- Channels with epileptic events show more total and outgoing propagations in the ripple, gamma, and theta bands than channels without
- Epileptic tissue acts as an outward hub up to the (fast) ripple frequency range
- The total strength in the gamma band seems to be a promising biomarker to delineate epileptic tissue intraoperatively

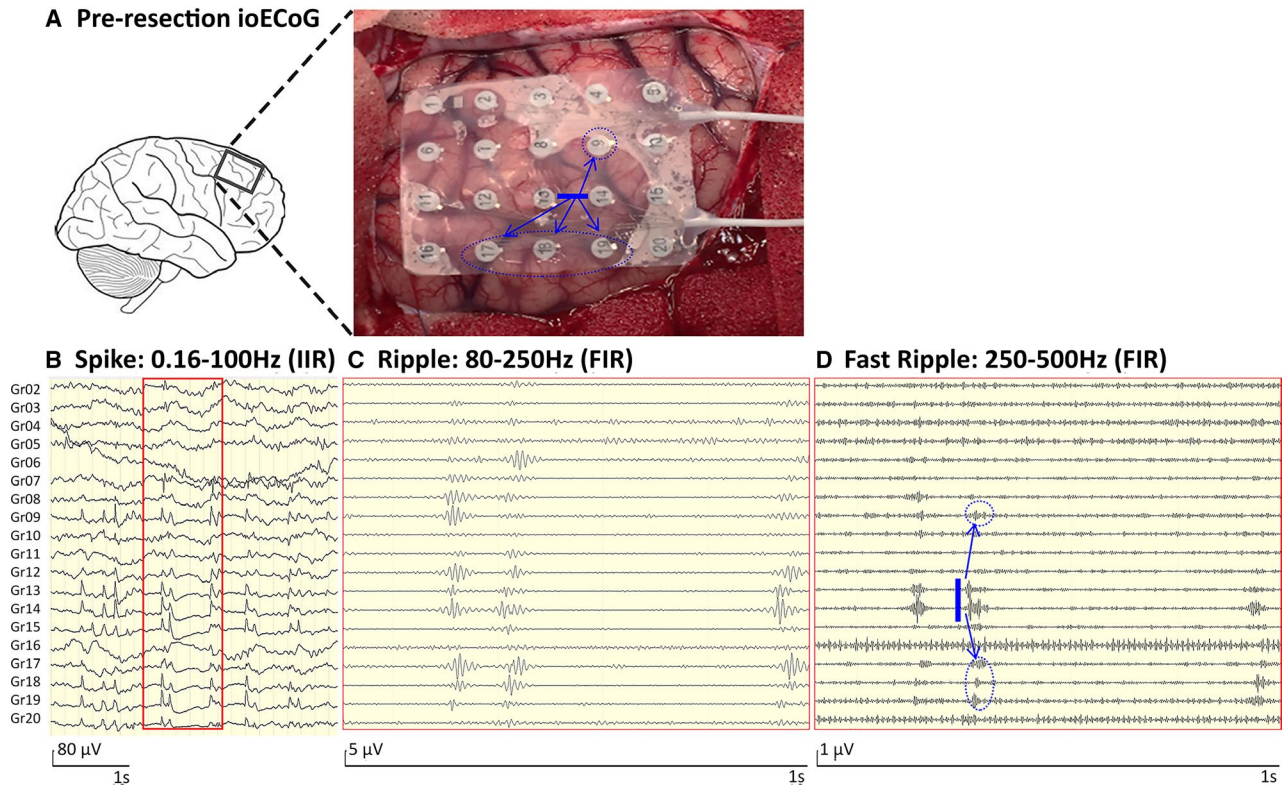

FIGURE 1 Example showing the propagation of high-frequency oscillation (HFO) activity in Patient 7. A, Preresection intraoperative electrocorticographic (ioECoG) recording situation in Patient 7. B, Four seconds of ioECoG in spike settings (infinite impulse response [IIR] filter: 0.16-100 Hz). Spikes are visible on electrodes 7-9, 12-15, and 17-20. C, One second of ioECoG in ripple settings (finite impulse response [FIR] filter: 80-250 Hz). Shown are ripples on electrodes 8, 9, 12-14, and 17-19. D, One second of ioECoG in fast ripple settings (FIR filter: 250-500 Hz). Fast ripples seem to propagate from electrodes 13-14 across a distinct but still spatially confined cortical area (to electrodes 9, 17-19). This is indicated by the blue arrows and could be the silhouette of an underlying HFO-generating network

2 | MATERIALS AND METHODS

2.1 | Patient selection

Figure 2 shows the patient selection flowchart. We aimed to include patients in whom the epileptic tissue was covered by ECoG electrodes and subsequently completely removed. We selected patients with a malformation of cortical development or brain tumor World Health Organization grade I/II, and at least three electrode contacts covering the resected area, from a retrospective database of refractory epilepsy patients who underwent ioECoG-tailored resective surgery at the University Medical Center in Utrecht, the Netherlands, between 2008 and 2012.[5] The database was collected following the guidelines of the institutional ethical committee. Patients with mesiotemporal pathologies were excluded, as the epileptogenic tissue may not be fully covered. Subtemporal, intraventricular, or interhemispheric strips were discarded, because the exact relation to the resected area was difficult to determine (Section 2.5). We compared patients who became seizure-free (Engel = IA) to those who did not become seizure-free (Engel ≥ IB).

2.2 | Data acquisition

IoECoG was recorded using 4 × 4, 4 × 5, or 4 × 8 electrode grids (Ad-Tech) placed directly on the cortex. The grids consist of platinum electrodes, embedded in silicon, with a contact surface of 4.2 mm^2 and an interelectrode distance of 1 cm. Recordings were made with a 64-channel EEG system (MicroMed) at a 2048-Hz sampling rate with a 538-Hz antialiasing filter. The signal was referenced to an external electrode placed on the mastoid. Grids were placed in multiple locations to ensure full sampling of the lesion and surrounding tissue.

Propofol infusion was interrupted during registration, until a continuous ioECoG background pattern was achieved. This enabled better detection and interpretation of interictal spikes for surgical decision-making.

2.3 | Data selection and preprocessing

We used the first, preresection ioECoG recording that met the inclusion criteria in each patient. It was not possible to select an equal set of epochs with or without events for all

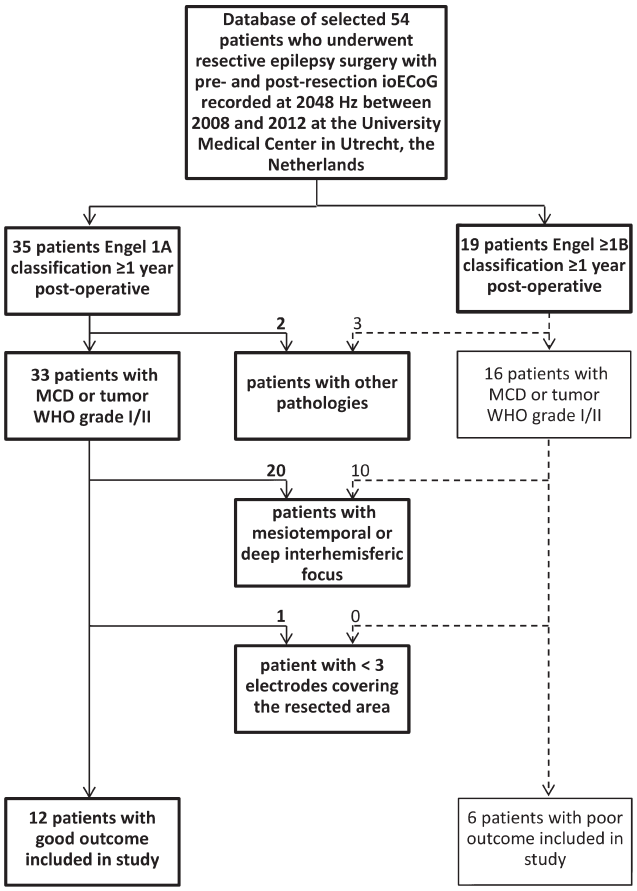

FIGURE 2 Flowchart patient selection. ioECoG, intraoperative electrocorticography; MCD, malformation of cortical development; WHO, World Health Organization grade

patients for functional network analysis. We therefore chose to minimalize the influence of selection bias,[32] and used the first four artifact-free epochs of 2 seconds. We started epoch selection at the end of the recording to assure minimal effect of propofol on HFOs and network measures.[33] We visually checked the epochs used for network analysis for spikes, ripples, and FRs (Section 2.6).

Two of the six patients with poor outcome had a second focus that was recorded during surgery, but too far away to extend the resection. We separately analyzed these two post-resection recordings.

Offline preprocessing of the data was performed using MATLAB. Channels containing noise were removed. We limited preprocessing steps to those useful for achieving data stationarity.[34] A zero-phase 1-Hz high-pass filter and notch filter were applied to detrend the signal and reduce possible contamination of 50-Hz noise. We took the z score of the signals by subtraction of the mean and division by the standard deviation. This was done to solve scaling issues between electrodes, which may result in erroneous calculation of functional connectivity.[15,26]

2.4 | Functional network analysis

Directed functional connectivity was computed for each epoch using the short-time direct directed transfer function (SdDTF).[35] The SdDTF is based on the concept of Granger causality, transferred to the frequency domain. Signal $x(t)$ has a Granger causal effect on $y(t)$ when adding the past of $x(t)$ improves the prediction of signal $y(t)$. To evaluate this causality in multichannel data, a multivariate autoregressive (MVAR) model is fitted to the recorded signals. Such a model assumes that the value of x at time t depends on the p past values of the signal itself, the p past values of signals at other electrodes and a random component. The model order (p) determines the size of the prediction window. We computed MVAR models with different orders (Section 2.7) using the modified least squares algorithm.[36]

The MVAR model is subsequently transformed to the frequency domain. The elements of the transfer matrix $H_{ij}(f)$ describe the causal flow from channel j to i at frequency f. This nonnormalized DTF is directly related to the coupling strength. The SdDTF is a variant of the DTF that is normalized to all propagations between all channels in the predefined frequency interval.[37] This enables comparison between epochs and subjects. In addition, the SdDTF distinguishes direct from indirect interactions by a multiplication with the partial coherence ($\chi_{ij}(f)$). The SdDTF is defined as

$$\zeta_{ij}(f) = \frac{|H_{ij}(f)||\chi_{ij}(f)|}{\sqrt{\sum_f \sum_{ij} |H_{ij}(f)|^2 |\chi_{ij}(f)|^2}}.$$

A nonzero SdDTF indicates direct causal interactions between signals in a multichannel recording at a certain frequency. The rows in the SdDTF adjacency matrix denote the inflow; the columns denote the outflow. We put the diagonal to zero, thereby eliminating self-connections. When two time series contain the same signal, there is no information flow between them, and the SdDTF should be zero.[38] We evaluated the gamma (30-80 Hz), ripple (80-250 Hz), and FR bands (250-500 Hz), because we aimed to reveal the propagation of high-frequency activity. We added the theta band (4-8 Hz) for comparison with existing literature. SdDTF calculation was performed using the SIFT toolbox.[39]

Per epoch, we determined node importance by calculating the total, instrength, and outstrength of each node. A nodes' total strength is the sum of the weights of the edges connected to this node.[15] A high strength means many and/or strong propagations to other nodes. In networks based on directed connectivity measures, the strength can be divided into in- and outstrength: the sum of all incoming and outgoing propagations. Nodes with a high strength are called hub nodes. In the case of directed

connectivity, these can be classified into sinks/receivers (high instrength) and sources/drivers (high outstrength).

2.5 | Resected area

The position of electrodes on the cortical surface in relation to the lesion and resected tissue was determined from photographs taken during surgery. Electrodes were classified into resected or nonresected.[4]

2.6 | Epileptic events

We extracted information about the epileptic activity that guided the resection from the clinical neurophysiological report of the surgery. We visually checked the epochs for presence of spikes, ripples, and FRs.[5]

2.7 | Model order selection

The model order determines the size of the prediction window of the MVAR model: the number of samples in the past that are taken into account. The Schwarz's Bayesian criterion (SBC) and Akaike's final prediction error (FPE) are common algorithms used to determine the optimal model order. They are built on the model fit to the data, and try to determine a tradeoff between bias and variance: finding the order with the smallest residual (ie, best fit), while reducing overfitting by means of a penalty term. Applying the SBC resulted in a median optimal model order of 4 for all patients, and the FPE of 7.5. We reasoned that at least one cycle of the frequency of interest is needed for accurate modeling, and therefore decided to compute MVAR models with orders of 4, 10, 20, 30, and 68. We first objectively determined which model order best predicted whether a channel was part of the resected area and whether a channel was showing events using the area under the receiver operating characteristic (ROC) curves for each frequency band. Model fitting to the high-frequency ranges is challenging, because high-frequency activity has very little impact on the residuals. We therefore visually validated the model orders using data from the example patient in Figure 1, and simple FR simulations. We assessed stationarity of the time series in each epoch using the augmented Dickey-Fuller tests, and stability of the fitted MVAR models using the autocorrelation function, Portmanteau tests, and stability index.

2.8 | Statistical analyses

We compared patient characteristics between the good and poor outcome group using Mann-Whitney *U* (MWU) and Fisher exact tests. We used the mean total, instrength, and outstrength of every node over four epochs for analysis. We compared the total, instrength, and outstrength between nodes covering the resected and nonresected areas, and nodes with and without events in each patient using MWU tests. At the group level, we performed paired *t* tests between median strength values of channels covering the resected and nonresected areas of patients in the good and poor outcome group separately, and channels with and without events in patients with events. We used median values, because MWU testing is also based on the median values of the nodes in the resected and nonresected areas in each patient, and the number of electrodes was relatively small, so outliers would have a large impact when using the mean. All calculations were performed separately for each frequency band. A P value $< .05$ was considered significant.

For the network measure yielding the highest area under the curve overall, we calculated the positive and negative predictive value, sensitivity, and specificity for identifying the resected area in the good and poor outcome group, and for identifying channels showing spikes, ripples, and FRs in patients with the respective events for three thresholds: mean + ½ SD, mean + SD, and mean + 2 SD.

3 | RESULTS

Eighteen patients from our database were eligible for this study (Figure 2). Twelve had good and six had poor (Engel ≥ IB) seizure outcome at least 1 year after surgery. Median age at surgery and epilepsy duration did not differ between the groups: $age_{good} = 12$ (range = 1-41), $age_{poor} = 12.5$ (range = 3-44) years, $P = .80$; $duration_{good} = 4$ (range = 1-40), $duration_{poor} = 1.5$ (range = 0.1-19) years, $P = .25$. The location of the epilepsy was significantly different: in the good outcome group, the epilepsy predominantly involved the temporal and frontal lobes; in the poor outcome group, the (parieto)central regions ($P = .05$). Left and right hemisphere were equally represented. The distribution of patients with tumors or malformations of cortical development as underlying pathology did not differ between groups ($P = 1.0$); neither did the fraction of patients showing epileptic activity in their preresection ioECoG recording ($P = 1.0$) or in the analyzed epochs ($P = .15$; Table 1).

All channels in all epochs contained stationary data. Figure S1 shows ROC curves of all combinations of directed strength measure, frequency band, and model order in predicting whether a channel was part of the resected area, and whether a channel was showing epileptic events. All MVAR models met the criteria of stability. A model order of 4 yielded the highest areas under the curves for directed strength measures in the FR band, a model order of 10 in the ripple band, and a model order of 68 in the gamma and theta bands. In the ripple, gamma, and theta bands, the different model orders resulted in similar ROC curves; in the FR band, the model order really influences the shape of the curve. Visually checking the model orders using patient

TABLE 1 Patient characteristics

Pt	Sex	Age surgery, y	Epilepsy duration	Side	Location	Pathology	Follow-up, mo	Engel class	AED free	Channels, n	Resected channels, n	Spikes in ioECoG overall	Epochs with Sp/Ri/FR, n
1	F	1	1 y	L	TO	GM WHO II	18	IA	Yes	17	13	Spikes Gr3, 4, 6-8, 11-14, 18-19	2/0/0
2	F	3	2 y	L	T	GGM WHO I	30	IA	Yes	17	13	Sharp waves Gr6-8, 16, 18, 19; bursts Gr18	0/0/0
3	M	8	8 y	L	Fr	FCD 2A	31	IA	Yes	18	10	—	0/0/0
4	M	9	8 y	R	Fr	FCD 2B~	32	IA	Yes	31	16	Spikes Gr1, 2, 9, 17, 20, 26, 27	4/3/0
5	F	12	1 y	L	Fr	FCD 2A	38	IA	Yes	15	10	Spikes Gr2-5, 7-10, 12	3/1/0
6	M	12	1 y	R	Fr	DNET WHO I	49	IA	Yes	17	4	—	0/0/0
7	M	14	12 y	R	Fr	FCD 2B	25	IA	Yes	16	10	Continuous Gr8-10, 12-15, 17-20	4/4/4
8	M	16	2 y	L	T	GGM WHO II	25	IA	Mono	16	10	Spikes Gr2-4, 6-8, 10	0/0/0
9	M	17	5 y	R	T	FCD 2B	12	IA	Yes	18	4	Bursts Gr7-9, 12-14, 19	3/2/2
10	F	20	5 y	R	T	PXA WHO II	15	IA	Yes	18	7	—	0/0/0
11	M	41	40 y	R	Fr	FCD 2B	36	IA	Yes	19	6	Spikes Gr1, 2, 6, 7, 11	0/0/0
12	F	5	3 y	R	Fr	FCD 2B~	20	IA	Mono	15	8	Bursts Gr6, 7, 12, 13	0/0/0
13	M	11	3 y	R	C	mMCD II	57	IVB	Poly	20	9	Bursts Gr2-4, 7, 8, 12-15, 17-20	3/3/3
14	M	12	1 y	R	Fr	GGM WHO I	79	IIA	Mono	17	3	—	0/0/0
15	M	44	19 y	R	PC	mMCD II	53	IVB	Poly	20 (+20)	10 (0)	Continuous Gr6-8, 10, 12-14, 17-18 (Continuous Gr1, 10, 12, 18)	4/4/4 (4/4/4)
16	M	14	2 y	L	C	DNET WHO I	87	IB	Yes	19	4	Spikes Gr7, 8, 10, 12, 13, 16, 17	4/4/1
17	M	13	1 y	L	P	FCD 2B~	40	IVB	Poly	20 (+18)	9 (0)	Continuous Gr7-15, 19, 20 (Continuous Gr12-14, 16-18)	4/4/4 (4/4/4)
18	F	3	6 wk	L	T	FCD 1A	12[a]	IIIA	Mono	20	8	Spikes Gr1-3, 6-9, 12-14, 18, 19	4/4/2

Note. Numbers in parentheses represent numbers of channels and resected channels in postresection recording.

Abbreviations: ~, in the context of tuberosclerosis complex; AED, antiepileptic drug; C, central; DNET, dysembryoplastic neuroepithelial tumor; F, female; FCD, focal cortical dysplasia; FR, fast ripple; Fr, frontal; GGM, ganglioglioma; GM, glioma; ioECoG, intraoperative electrocorticography; L, left; M, male; mMCD, mild malformation of cortical development; P, parietal; PC, parieto-central; Pt, patient; PXA, pleomorphic xanthoastrocytoma; R, right; Ri, ripple; Sp, spike; T, temporal; TO, temporo-occipital; WHO, World Health Organization grade.

[a]This patient had a hemispherectomy 1 year after the first surgery and became seizure-free afterward.

data shows that a model order of 4 grasps the propagation between channels with FRs, but when integrating over the frequency band, the connectivity is not strong enough to discriminate it from the connectivity between channels without events (Figure 3). There is a difference in connectivity strength between channels with and without FR from model order 20 onward. Based on simple FR simulations, you would need a model order of at least 10 to start to see the "bump" in the SdDTF propagation of channels with FRs (Figure S2). In the ripple to theta bands, model orders 4-30 showed connectivity between the channels showing events. In all frequency bands, the model started to overfit the background/powerline artifacts at model order 68. Based on these results, we used a model order of 30 for all frequency bands in the analyses that follow.

Figure 4 summarizes the combined group- and patient-level results for the comparison of network measures between channels covering the resected and nonresected areas and channels with and without epileptic activity in the ioECoG overall. Channels covering the resected area in patients with good outcome show a higher total and outstrength in the ripple and gamma bands than channels covering the nonresected area. In the gamma band, there is also a trend toward a higher instrength. Channels covering the resected area in patients with poor outcome show a higher instrength in the theta band. Channels with events in the ioECoG overall show a lower total and instrength, and higher outstrength in the FR band, a higher outstrength in the ripple band, a higher total, instrength, and outstrength in the gamma band, and a higher total and outstrength in the theta band than channels without events.

Of all strength measures, the total strength in the gamma band appeared to be the best predictor at the channel level (area under the curve $[AUC]_{Res/nRes} = 0.57$, 95% confidence interval [CI] = 0.49-0.64, $P = .07$; $AUC_{Ev/nEv} = 0.79$, 95% CI = 0.74-0.84, $P < .001$; Figure S1). This measure is also most often significant at the patient level (Figure 4). Electrodes with gamma total strength above the mean + SD threshold can be identified in all patients, and are most often included in the resected area in patients with good seizure outcome (26 of 35 identified electrodes resected), but not in patients with poor seizure outcome (five of 14 identified electrodes resected; Figure 5 and Figure S3). This threshold yields a positive predictive value (PPV) of 74% and 43% for identifying the resected area in patients with good or poor outcome, respectively, and a PPV of 93%, 92%, 85%, and 66% for identifying channels showing events in the ioECoG overall, and channels with spikes, ripples, and FRs in the analyzed epochs (Table S4).

The method showed significant results in patients with epileptic activity in the epochs used for network analysis; in patients without epileptic activity in their epochs, but elsewhere in the ioECoG recording (Patients 2, 11, and 12); and in a patient without events in the ioECoG overall, but a clear epileptic underlying substrate (focal cortical dysplasia 2A, Patient 3). The method did not work in the three patients with a tumor without epileptic activity in their ioECoG recording (Patients 6, 10, and 14).

4 | DISCUSSION

Based on the observation of HFOs "spreading out" from the epileptic source, we aimed to distinguish epileptic from healthy brain tissue using measures of directed connectivity in the high-frequency bands. We compared values of total, instrength, and outstrength in the high-frequency ranges of ioECoG recordings between electrodes covering the resected and nonresected areas separately for lesional focal epilepsy patients who did and did not become seizure-free after surgery, and between electrodes with and without spikes, ripples, and FRs. In patients with good outcome, channels covering resected tissue showed a higher total and outstrength in the ripple and gamma bands than channels covering nonresected tissue. In patients with poor outcome, channels covering the resected area showed a higher instrength in the theta band. Channels with events showed a lower total and instrength and higher outstrength in the FR band, a higher outstrength in the ripple band, a higher total, instrength, and outstrength in the gamma band, and a higher total and outstrength in the theta band than channels without events. The epileptic tissue thus seems isolated in the FR frequency range and acts as an "outward" hub up to the (fast) ripple frequency range. The total strength in the gamma band seems to be a promising measure to delineate the epileptic tissue intraoperatively, even in the absence of interictal spikes and HFOs in the analyzed epochs, but not in patients with a tumor as underlying pathology and no epileptic activity measured in the ioECoG.

Our results are in line with previous studies investigating directed functional connectivity in intracranial EEG of patients with focal epilepsy that found functional isolation of presumed epileptic tissue in the high-frequency ranges,[21,23,27] and increased outstrength from the epileptic tissue in the conventional frequency ranges.[20,24–26,31] The finding of theta and gamma connectivity flow in the same direction makes sense given the strong theta-gamma coupling.[40] The decreased total and instrength, and increased outstrength in the FR band of channels showing events may delineate the epileptogenic core, which is functionally isolated interictally, but becomes more connected during seizure progression, and from where interictal discharges spread when suppression fails.[28]

A limitation in studies aiming to identify the epileptic tissue is the lack of an unambiguous marker. Epileptic tissue is defined as the clinically determined SOZ,[23,26,41] areas showing low-voltage rapid discharges,[31] areas with evident FR activity,[23,27] and the surgically resected tissue in the case of

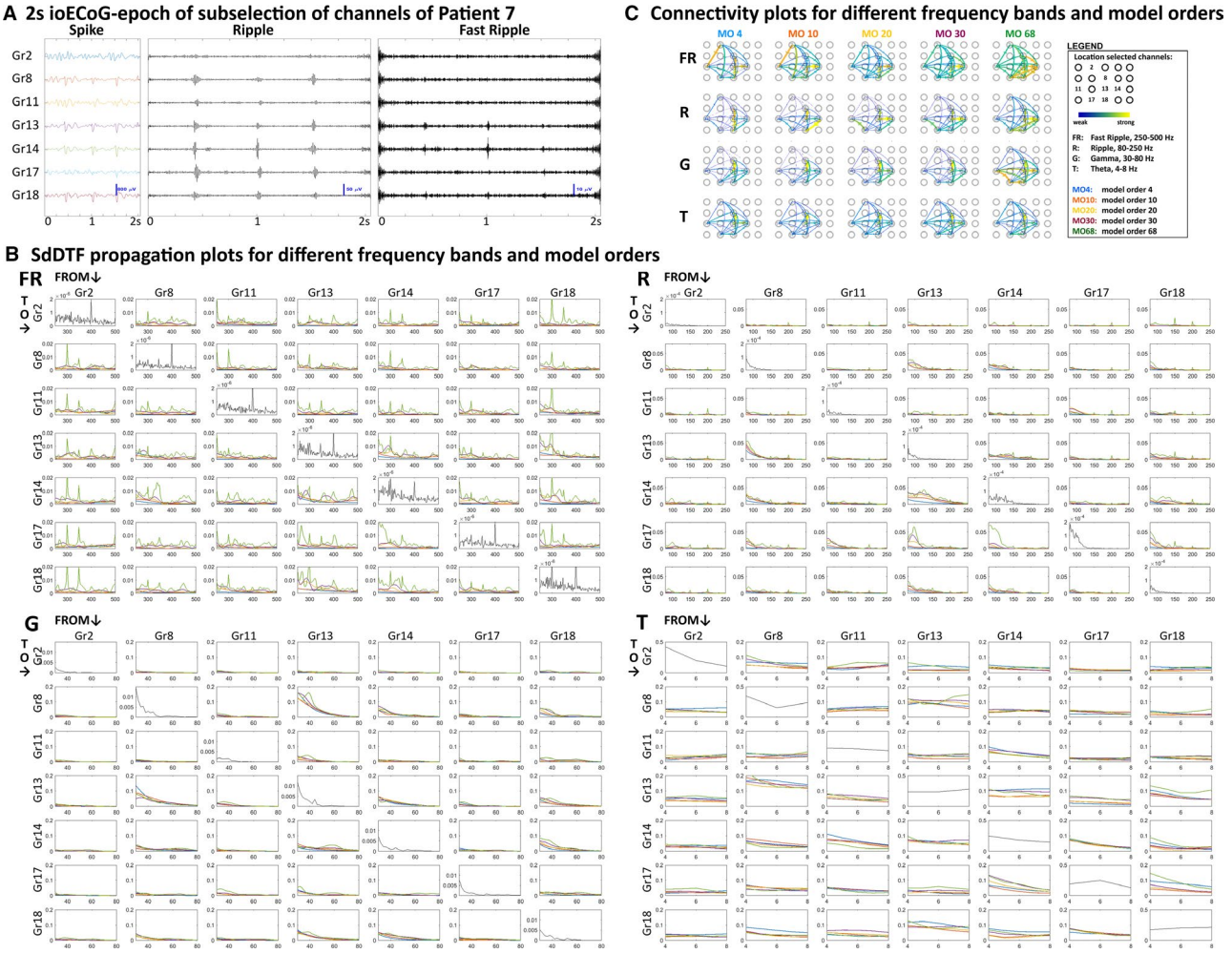

FIGURE 3 Short-time direct directed transfer function (SdDTF) propagation and connectivity plots for different frequency bands and model orders (MOs) in selected channels of epoch 1 of example Patient 7. A, Two-second epoch of intraoperative electrocorticography (ioECoG) in a subselection of channels of example Patient 7 in spike (infinite impulse response filter: 0-100 Hz), ripple (finite impulse response [FIR] filter: 80-250 Hz), and fast ripple (FR; FIR filter: 250-500 Hz) settings. The ioECoG shows FRs in Gr13 and Gr14, ripples in Gr8, Gr13, Gr14, Gr17, and Gr18, and spikes in the same channels as ripples. B, SdDTF propagation plots for the FR, ripple (R), gamma (G), and theta (T) frequency bands. Each off-diagonal plot shows the SdDTF propagation from the channel indicated above the column to the channel marked before the row for different MOs (blue = MO 4, orange = MO 10, yellow = MO 20, purple = MO 30, green = MO 68). The columns thus represent the outgoing SdDTF connectivity strength of the channels, and the rows represent the incoming connectivity strength. The diagonal plots show the power spectra of the channels. In the FR band, starting from MO 4, we see a "bump" in the SdDTF propagation plots of the channels showing FRs (Gr13, Gr14, and to a lesser extent Gr18). At MO 68, the model overfits harmonics of the powerline artifact, and the difference between channels with and without events becomes less clear. In the ripple band, there is a clear SdDTF flow between Gr8, Gr13, and Gr14, starting at MO 4. From MO 10 onward, there is also SdDTF propagation to Gr17 and Gr18, which also shows ripple events. The model starts to overfit the harmonics of the powerline artifact at MO 68. In the gamma band, there is a clear SdDTF flow between Gr8, Gr13, Gr14, and Gr18, the channels showing events, for all MOs. In the theta band, the SdDTF shows less clear results, but does identify a strong connection between Gr8 and Gr13. In the theta and gamma bands, different MOs yield similar propagation plots, with slightly more detail with increasing MO. C, Integrated SdDTF propagation for different frequency bands (rows) and MOs (columns) projected on a grid. Within each subplot, connections are normalized to the strongest connection. In the FR band, the connections between Gr13, Gr14, and Gr18, the channels with events, are between the strongest connections for all MOs. At MOs 4 and 10, there also exists a strong connection between Gr2 and Gr11, two channels not showing FRs. From MO 20 onward, the connection between Gr13 and Gr14 is clearly stronger than the connection between Gr 2 and Gr11. At MO 68, the overall connectivity strength is higher over the whole grid, and there appear strong connections between channels showing clear FRs and their neighboring electrodes. In the ripple band, similar to the SdDTF propagation plots, the connections to Gr17 and Gr18 start to get stronger from MO 10 onward. At MO 68, the overall connectivity is higher, and the connection between Gr17 and Gr11 starts to disappear again. In the gamma band, MOs 4 to 30 provide similar connectivity plots, with the strongest connections between the channels showing events. At MO 68, the overall connectivity strength is higher. In the theta band, all MOs provide a similar connectivity plot, with the strongest connection between Gr8 and Gr13

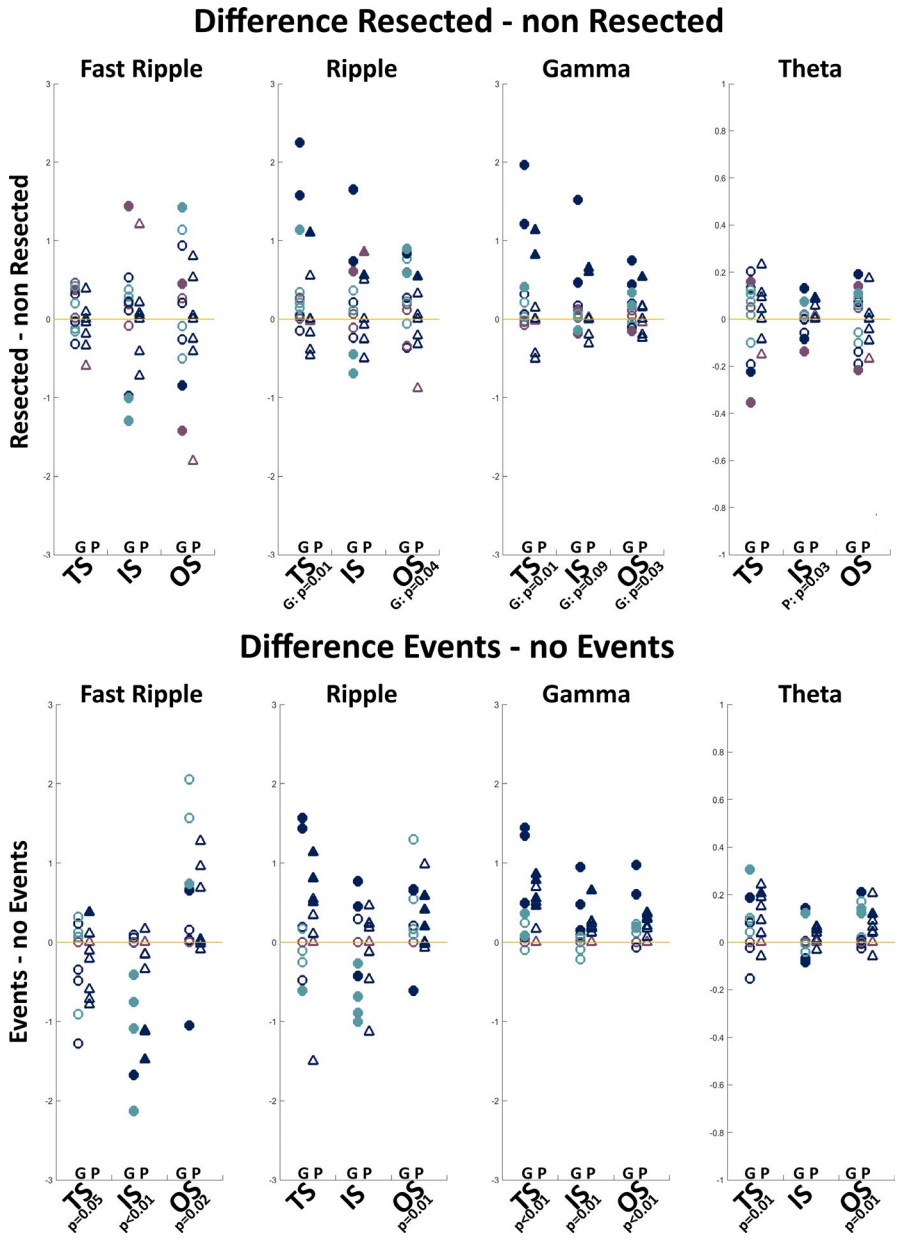

FIGURE 4 Difference in directed strength measures in the fast ripple, ripple, gamma, and theta bands between the resected and nonresected areas (upper) and between channels with and without events (lower). The difference between resected and nonresected areas or channels with and without events is calculated by subtracting the median value of the electrodes in the former group from the median value of the electrodes in the latter group in each patient. Positive values indicate a higher value and negative values indicate a lower value in resected/event channels than nonresected/nonevent channels. Colors indicate whether a patient had events in the epochs used for network analysis (dark blue), events in the overall intraoperative electrocorticography (ioECoG) recording but not in the analyzed epochs (light blue), or no events in the ioECoG at all (purple). Circles are patients with good (G) surgery outcome; triangles are patients with poor (P) surgery outcome. A filled symbol indicates a significant difference between the resected and nonresected areas or channels with and without events at the individual patient level. The given *P* values indicate significant difference at the group level. What can be seen is that channels covering the resected area in patients with good outcome show a higher total strength (TS) and outstrength (OS) in the ripple and gamma bands than channels covering the nonresected area. In the gamma band, there is also a trend toward a higher instrength (IS). Channels covering the resected area in patients with poor outcome show a higher IS in the theta band than channels not covering the resected area. Channels with events show a lower TS and IS, and higher OS in the fast ripple band, a higher OS in the ripple band, a higher TS, IS, and OS in the gamma band, and a higher TS and OS in the theta band than channels without events

postoperative seizure freedom.[24] We used the resected area, and channels showing spikes, ripples, and FRs. We compared values of epileptogenic to nonepileptogenic tissue in patients with good and poor postoperative outcome. In the good outcome group, the resected area likely also contains healthy tissue. In the poor outcome group, the nonresected

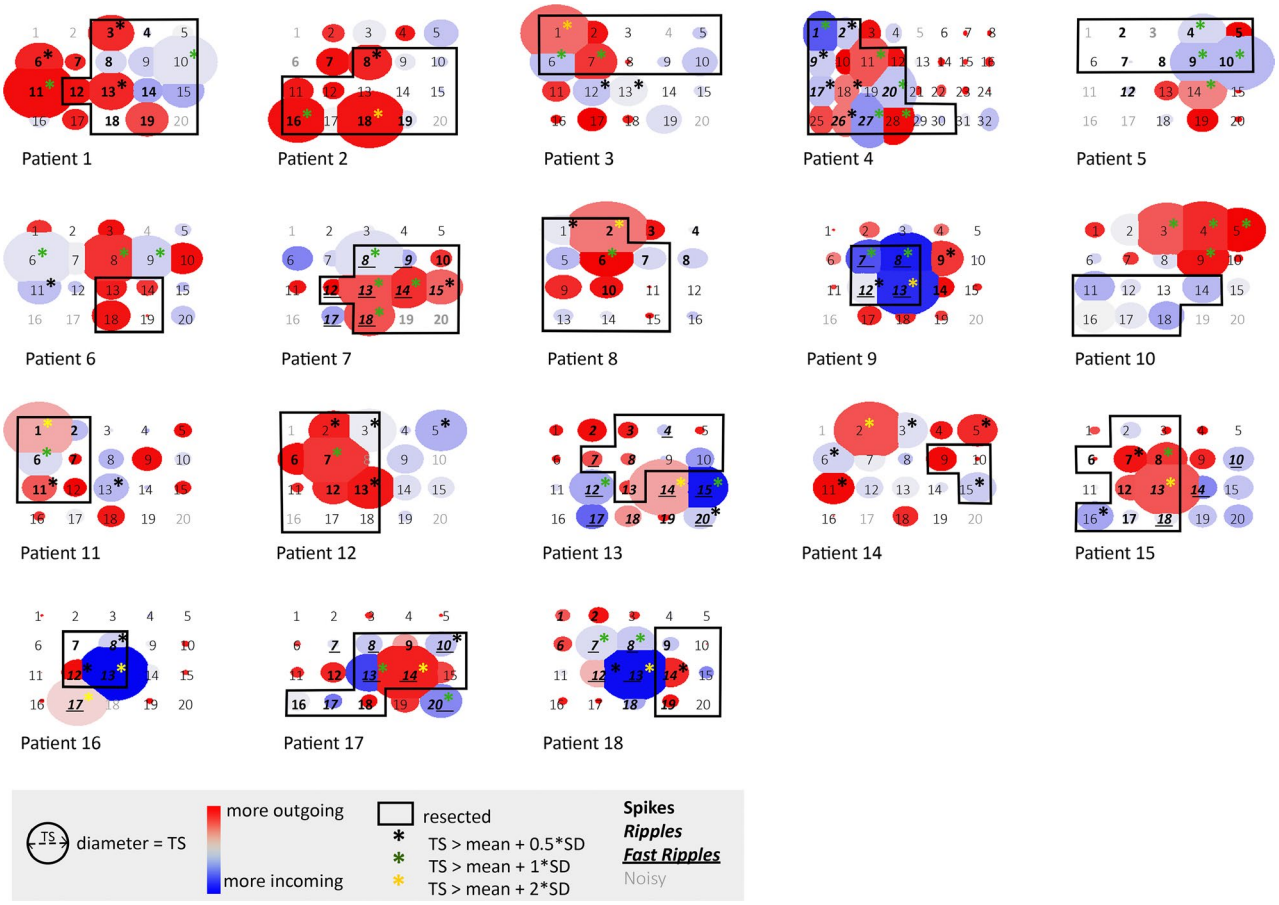

FIGURE 5 Schematic representation of the total strength in the gamma band for all cases (1-12 good outcome, 13-18 poor outcome). The size of the circle represents the value of the total strength in the gamma band. The color indicates whether there are more/stronger outgoing (red) or incoming (blue) propagations. The resection (black rectangle) was based on results of preoperative examinations and tailoring based on spikes in the intraoperative electrocorticogram (ioECoG). Asterisks indicate nodes that should be included in the resection based on three different thresholds (black: total strength [TS] > mean + 0.5 SD, good outcome: 40 of 56 identified electrodes, poor outcome: 12 of 27 identified electrodes resected; green: TS > mean + 1 SD, good outcome: 26 of 35 identified electrodes, poor outcome: five of 14 identified electrodes resected; yellow: TS > mean + 2 SD, good outcome: five of five identified electrodes, poor outcome: three of seven identified electrodes resected; it should be noted that only five of 12 good outcome, and six of six poor outcome patients had electrodes with a gamma band total strength above mean + 2 SD). Different font styles indicate whether electrodes showed no events (regular), spikes (bold), ripples (bold italics), or fast ripples (bold italics underlined) in the epochs analyzed for network analyses or were removed because of noise (gray). What can be seen is that electrodes with a gamma band total strength above mean + SD threshold can be identified in all patients, and are most often included in the resected area in patients with good seizure outcome (1-12) but not in patients with poor seizure outcome (13-18). These are predominantly the channels that show events. The above method does not rely on the presence of epileptic activity in the epochs analyzed for network analysis. Patients 2, 11, and 12 did not have epileptic activity in their epochs, but did elsewhere in the ioECoG recording. Patient 3 had no events in the ioECoG overall, but a clear epileptic underlying substrate (focal cortical dysplasia 2A). However, the method does not yield significant results in tumor patients without any epileptic activity in their ioECoG recording overall (Patients 6, 10, and 14)

area still contains epileptic tissue. The poor outcome patients included in this study had more complex epilepsies (ie, in/close to eloquent brain areas) and/or multiple foci that were not always recorded intraoperatively. This may have blurred the results. In the good outcome group, two patients were still undergoing withdrawal from antiepileptic drugs at the time of the latest available follow-up. Late recurrences can occur, especially during withdrawal of antiepileptic drugs, so in these patients the resected tissue might not be a solid marker. We classified electrodes as resected or nonresected based on photographs taken during surgery. However, it was sometimes difficult to determine whether an electrode was on the edge or part of the resected area. Instead of dichotomizing electrodes as resected or nonresected, one could use strength as a function of the Euclidean distance from the resection margin, especially if a single epileptic focus is suspected. We did not choose this option because our data included patients with tumors in whom one of the borders could encompass the epileptic tissue, so the distance from the resection does not necessarily represent the distance from the epileptic focus.

Another challenge is the influence of methodological choices in functional network analysis. The choice of connectivity measure, connectivity measure–associated parameters such as model order, montage, and options in preprocessing all affect results.[32] We chose the SdDTF as connectivity measure. The DTF is popular because it is robust to noise, performs well in case of nonlinear signals,[37] and can identify the correct underlying structure based on short data segments.[42] The choice of model order is important in MVAR-based measures like the SdDTF, as it determines the size of the prediction window. We used data-driven approaches that we visually validated with patient data (Figure 3) and simulations (Figure S2), because traditional model order selection paradigms build on the model fit to the data, and high-frequency activity has very small impact on the residuals. This resulted in a model order of 30. It is generally agreed that the number of data samples should be at least 10 times the number of parameters to obtain a proper fit, but it is uncertain whether this is a hard rule.[36,43] Based on this rule, orders > 20 should be treated with care. However, as the different model orders yielded similar propagation plots in the conventional frequency bands, with more detail with increasing model order, we deemed the results plausible. In the FR band, the outstrength seemed especially influenced by the model order; lower model orders resulted in decreased outstrength in the resected area or channels with events, whereas higher model orders led to increased outstrength, in particular when evaluating epochs containing events (Figure S1). This might indicate that with short prediction windows, the model is unable to capture the stochastic spreading epileptic activity but can model the background signal in nonepileptic channels, resulting in a higher connectivity between nonepileptic channels. The preprocessing steps necessary for MVAR-based connectivity measures are debated. We followed the methodology suggested by Barnett and Seth; we excluded artifacts, and limited filtering to improve stationarity. We removed drift and powerline noise by means of a 1-Hz high-pass and 50-Hz notch filter, but did not bandpass filter in the frequency range of interest before fitting an MVAR model, as this may corrupt MVAR model estimates.[34] Others argue that for an MVAR model to properly represent the data of interest, the high-amplitude activity below the frequency of interest should be filtered out. Choosing a reference is also a point of discussion in functional connectivity studies; some say rereferencing to common average reference (CAR) is necessary to increase the signal-to-noise ratio, whereas others argue that it induces a directionality.[16] Because MVAR fitting to the high-frequency ranges is not common, we assessed the influence of bandpass filtering and reference choice on MVAR model fitting on patient data and FR simulations (Figures S2, S5, S6). Rereferencing to CAR made the difference between channels with and without events fade in the conventional bands and disappear in the FR band; bandpass filtering prior to MVAR fitting induced strange peaks in the (high-frequency) SdDTF plots. Filtering sharp events, like artifacts and spikes, may produce false oscillations.[44,45] Artifacts typically occur at the same time over several channels (Figure S7). We do not expect these artifacts to influence results, because they show no spread and because we visually checked the epochs. Ripples and FRs predominantly occur before the peak of the spike and are thus not a filtering effect.[46] In addition, spikes are indicators of epileptogenic networks too. Therefore, spreading spikes, or spreading artifacts of filtered spikes, may help in distinguishing epileptogenic tissue.

Given the numerous tests performed, the issue of alpha error cumulation arises. We did not correct for multiple comparisons, because of the explorative nature of this study. The decreased FR instrength and increased gamma total and outstrength in channels with events would remain significant after Bonferroni correction for the number of network measures, frequency bands, and outcomes tested. We did not correct for the tests performed to address the influence of methodological choices (model order, reference type, bandpass filtering or not), because this was not the primary aim of the study.

To conclude, directed functional connectivity analysis in the high-frequency bands seems a promising method for the identification of epileptic tissue. Especially the total strength in the gamma band robustly showed high values in the resected areas or channels showing events irrespective of model order, filtering strategy, and montage used, and could be helpful during surgery. Epileptic activity is stochastic in nature. Given a truly epileptogenic underlying substrate, however, our method seems to be able to pinpoint the epileptic tissue even in the absence of events. Results need to be replicated in a larger patient group, including mesial epilepsies, to increase generalizability, and facilitate clinical implementation. A large methodological study should be performed investigating the optimal connectivity measure, network measure, and epoch length and number to identify functional network structure in different frequency ranges. High-frequency network analysis possibly benefits from high-density ECoG recordings and time-varying analysis in the millisecond range. A sliding window approach with short, highly overlapping windows and ensemble averaging or connectivity on the envelope of the oscillations could be used to study this properly.[47]

ACKNOWLEDGMENTS

W.J.E.M.Z. is supported by the UMC Utrecht Alexandre Suerman MD/PhD Stipendium 2015. M.A.v.t.K. was supported by the Dutch Epilepsy Foundation grant number 2012-04. N.E.C.v.K. is supported by the Dutch Brain Foundation grant number 2013-139 and the Dutch Epilepsy Foundation grant number 2015-09. M.Z. is supported by the ZonMW-VENI grant number 91615149. We thank our colleagues C. F. Ferrier, T. A. Gebbink, and P. H. Gosselaar at

the UMC Utrecht for their collaboration and clinical contributions; B. E. Mouthaan for his contribution to the intraoperative ECoG database; C. Papageorgakis of the DynaMap team at INSERM Marseille for creating the FR simulations; and the anonymous reviewers for constructive comments.

CONFLICT OF INTEREST

None of the authors has any conflict of interest to disclose. We confirm that we have read the Journal's position on issues involved in ethical publication and affirm that this report is consistent with those guidelines.

ORCID

Willemiek J. E. M. Zweiphenning https://orcid.org/0000-0002-0720-7878

Maeike Zijlmans https://orcid.org/0000-0003-1258-5678

REFERENCES

1. Lamberink HJ, Boshuisen K, Van Rijen PC, Gosselaar PH, Braun KP; Dutch Collaborative Epilepsy Surgery Program (DCESP). Changing profiles of pediatric epilepsy surgery candidates over time: a nationwide single-center experience from 1990 to 2011. Epilepsia. 2015;56:717–25.
2. Jacobs J, Staba R, Asano E, et al. High-frequency oscillations (HFOs) in clinical epilepsy. Prog Neurobiol. 2012;98:302–15.
3. Wu JY, Sankar R, Lerner JT, Matsumoto JH, Vinters HV, Mathern GW. Removing interictal fast ripples on electrocorticography linked with seizure freedom in children. Neurology. 2010;75:1686–94.
4. van Klink NEC, van't Klooster Ma, Zelmann R, et al. High frequency oscillations in intra-operative electrocorticography before and after epilepsy surgery. Clin Neurophysiol. 2014;125:2212–9.
5. van 't Klooster MA, van Klink NEC, Leijten FSS, et al. Residual fast ripples in the intraoperative corticogram predict epilepsy surgery outcome. Neurology. 2015;85:120–8.
6. Zijlmans M, Jacobs J, Zelmann R, Dubeau F, Gotman J. High-frequency oscillations mirror disease activity in patients with epilepsy. Neurology. 2009;72:979–86.
7. Jefferys JGR, Menendez de la Prida L, Wendling F, et al. Progress in neurobiology mechanisms of physiological and epileptic HFO generation. Prog Neurobiol. 2012;98:250–64.
8. Fink CG, Gliske S, Catoni N, Stacey WC. Network mechanisms generating abnormal and normal hippocampal high-frequency oscillations: a computational analysis. eNeuro. 2015;2:1–19.
9. Kramer MA, Cash SS. Epilepsy as a disorder of cortical network organization. Neuroscientist. 2012;18(4):360–72.
10. Stam CJ. Modern network science of neurological disorders. Nat Rev Neurosci. 2014;15:683–95.
11. Richardson MP. Large scale brain models of epilepsy: dynamics meets connectomics. J Neurol Neurosurg Psychiatry. 2012;83:1238–48.
12. Lehnertz K, Ansmann G, Bialonski S, Dickten H, Geier C, Porz S. Evolving networks in the human epileptic brain. Phys D Nonlinear Phenom. 2014;267:7–15.
13. Coito A, Genetti M, Pittau F, et al. Altered directed functional connectivity in temporal lobe epilepsy in the absence of interictal spikes: a high density EEG study. Epilepsia. 2016;57:402–11.
14. Bullmore E, Sporns O. Complex brain networks: graph theoretical analysis of structural and functional systems. Nat Rev Neurosci. 2009;10:186–98.
15. Rubinov M, Sporns O. Complex network measures of brain connectivity: uses and interpretations. Neuroimage. 2010;52:1059–69.
16. Bastos AMAM, Schoffelen J-M. A tutorial review of functional connectivity analysis methods and their interpretational pitfalls. Front Syst Neurosci. 2015;9:175.
17. Kida T, Tanaka E, Kakigi R. Multi-dimensional dynamics of human electromagnetic brain activity. Front Hum Neurosci. 2016;9:713.
18. Ponten SC, Bartolomei F, Stam CJ. Small-world networks and epilepsy: graph theoretical analysis of intracerebrally recorded mesial temporal lobe seizures. Clin Neurophysiol. 2007;118:918–27.
19. Kramer MA, Kolaczyk ED, Kirsch HE. Emergent network topology at seizure onset in humans. Epilepsy Res. 2008;79:173–86.
20. Wendling F, Chauvel P, Biraben A, Bartolomei F. From intracerebral EEG signals to brain connectivity: identification of epileptogenic networks in partial epilepsy. Front Syst Neurosci. 2010;4:154.
21. Ibrahim GM, Anderson R, Akiyama T, et al. Neocortical pathological high-frequency oscillations are associated with frequency-dependent alterations in functional network topology. J Neurophysiol. 2013;110:2475–83.
22. Epstein CM, Adhikari BM, Gross R, Willie J, Dhamala M. Application of high-frequency Granger causality to analysis of epileptic seizures and surgical decision making. Epilepsia. 2014;55:2038–47.
23. Van Diessen E, Hanemaaijer JI, Otte WM, et al. Are high frequency oscillations associated with altered network topology in partial epilepsy? Neuroimage. 2013;82:564–73.
24. Wilke C, Worrell G, He B. Graph analysis of epileptogenic networks in human partial epilepsy. Epilepsia. 2011;52:84–93.
25. Varotto G, Tassi L, Franceschetti S, Spreafico R, Panzica F. Epileptogenic networks of type II focal cortical dysplasia: a stereo-EEG study. Neuroimage. 2012;61:591–8.
26. van Mierlo P, Carrette E, Hallez H, et al. Ictal-onset localization through connectivity analysis of intracranial EEG signals in patients with refractory epilepsy. Epilepsia. 2013;54:1409–18.
27. Zweiphenning WJEM, van 't Klooster MA, van Diessen E, et al. High frequency oscillations and high frequency functional network characteristics in the intraoperative electrocorticogram in epilepsy. Neuroimage Clin. 2016;12:928–39.
28. Burns SP, Santaniello S, Yaffe RB, et al. Network dynamics of the brain and influence of the epileptic seizure onset zone. Proc Natl Acad Sci U S A. 2014;111:E5321–30.
29. Ortega GJ, Sola RG, Pastor JJ. Complex network analysis of human ECoG data. Neurosci Lett. 2008;447:129–33.
30. Korzeniewska A, Cervenka MC, Jouny CC, et al. Ictal propagation of high frequency activity is recapitulated in interictal recordings: effective connectivity of epileptogenic networks recorded with intracranial EEG. Neuroimage. 2014;101:96–113.
31. Courtens S, Colombet B, Trebuchon A, Brovelli A, Bartolomei F, Bénar CG. Graph measures of node strength for characterizing preictal synchrony in partial epilepsy. Brain Connect. 2016;6:530–9.
32. van Diessen E, Numan T, van Dellen E, et al. Opportunities and methodological challenges in EEG and MEG resting state functional brain network research. Clin Neurophysiol. 2015;126:1468–81.

33. Zijlmans M, Huiskamp GM, Cremer OL, Ferrier CH, van Huffelen AC, Leijten FS. Epileptic high-frequency oscillations in intraoperative electrocorticography: the effect of propofol. Epilepsia. 2012;53:1799–809.
34. Barnett L, Seth AK. Behaviour of Granger causality under filtering: theoretical invariance and practical application. J Neurosci Methods. 2011;201:404–19.
35. Korzeniewska A, Crainiceanu CM, Kuś R, Franaszczuk PJ, Crone NE. Dynamics of event-related causality in brain electrical activity. Hum Brain Mapp. 2008;29:1170–92.
36. Schlögl A, Supp G. Analyzing event-related EEG data with multivariate autoregressive parameters. Prog Brain Res. 2006;159:135–47.
37. Blinowska KJ. Review of the methods of determination of directed connectivity from multichannel data. Med Biol Eng Comput. 2011;49:521–9.
38. Kamiński M, Ding M, Truccolo WA, Bressler SL. Evaluating causal relations in neural systems: Granger causality, directed transfer function and statistical assessment of significance. Biol Cybern. 2001;157:145–57.
39. Delorme A, Mullen T, Kothe C, et al. EEGLAB, SIFT, NFT, BCILAB, and ERICA: new tools for advanced EEG processing. Comput Intell Neurosci. 2011;2011:130714.
40. Canolty RT, Edwards E, Dalal SS, et al. High gamma power is phase-locked to theta oscillations in human neocortex. Science. 2006;313:1626–8.
41. Korzeniewska A, Franaszczuk PJ, Crainiceanu CM, Kuś R, Crone NE. Dynamics of large-scale cortical interactions at high gamma frequencies during word production: event related causality (ERC) analysis of human electrocorticography (ECoG). Neuroimage. 2011;56:2218–37.
42. Wang HE, Bénar CG, Quilichini PP, Friston KJ, Jirsa VK, Bernard C. A systematic framework for functional connectivity measures. Front Neurosci. 2014;8:1–22.
43. Höller Y, Uhl A, Bathke A, et al. Reliability of EEG measures of interaction: a paradigm shift is needed to fight the reproducibility crisis. Front Hum Neurosci. 2017;11:441.
44. Benar CG, Chauviere L, Bartolomei F, Wendling F. Pitfalls of high-pass filtering for detecting epileptic oscillations: a technical note on "false" ripples. Clin Neurophysiol. 2010;121:301–10.
45. Amiri M, Lina J, Pizzo F, Gotman J. High frequency oscillations and spikes: separating real HFOs from false oscillations. Clin Neurophysiol. 2016;127:187–96.
46. van Klink N, Frauscher B, Zijlmans M, Gotman J. Relationships between interictal epileptic spikes and ripples in surface EEG. Clin Neurophysiol. 2016;127:143–9.
47. Ding M, Bressler SL, Yang W, Liang H. Short-window spectral analysis of cortical event-related potentials by adaptive multivariate autoregressive modeling: data preprocessing, model validation, and variability assessment. Biol Cybern. 2000;83:35–45.

SUPPORTING INFORMATION

Additional supporting information may be found online in the Supporting Information section at the end of the article.

How to cite this article: Zweiphenning WJEM, Keijzer HM, van Diessen E, et al. Increased gamma and decreased fast ripple connections of epileptic tissue: A high-frequency directed network approach. *Epilepsia*. 2019;60:1908–1920. https://doi.org/10.1111/epi.16296